Monthly Notices of the ROYAL ASTRONOMICAL SOCIETY

MNRAS **519,** 3611–3622 (2023) https://doi.org/10.1093/mnras/stac3543
Advance Access publication 2022 December 9

A comparative analysis of the chemical compositions of Gaia-Enceladus/Sausage and Milky Way satellites using APOGEE

Laura Fernandes,[1] Andrew C. Mason,[1] Danny Horta ,[1] Ricardo P. Schiavon ,[1]★ Christian Hayes,[2] Sten Hasselquist,[3] Diane Feuillet ,[4] Rachael L. Beaton,[5,6] Henrik Jönsson,[7] Shobhit Kisku,[1] Ivan Lacerna ,[8,9] Jianhui Lian ,[10] Dante Minniti[11,12] and Sandro Villanova[13]

[1]*Astrophysics Research Institute, Liverpool John Moores University, 146 Brownlow Hill, Liverpool L3 5RF, UK*
[2]*NRC Herzberg Astronomy and Astrophysics, 5071 West Saanich Road, Victoria, BC V9E 2E7, Canada*
[3]*Space Telescope Science Institute, 3700 San Martin Drive, Baltimore, MD 21218, USA*
[4]*Lund Observatory, Department of Astronomy and Theoretical Physics, Box 43, SE-221 00 Lund, Sweden*
[5]*Department of Astrophysical Sciences, 4 Ivy Lane, Princeton University, Princeton, NJ 08544, USA*
[6]*The Observatories of the Carnegie Institution for Science, 813 Santa Barbara St, Pasadena, CA 91101, USA*
[7]*Materials Science and Applied Mathematics, Malmö University, SE-205 06 Malmö, Sweden*
[8]*Instituto de Astronomía y Ciencias Planetarias, Universidad de Atacama, Copayapu 485, Copiapó, Chile*
[9]*Millennium Institute of Astrophysics, Nuncio Monsenor Sotero Sanz 100, Of. 104, Providencia, Santiago, Chile*
[10]*Department of Physics and Astronomy, University of Utah, 115 S. 1400 E., Salt Lake City, UT 84112, USA*
[11]*Departamento de Ciencias Físicas, Facultad de Ciencias Exactas, Universidad Andres Bello, Fernández Concha 700, Las Condes, Santiago, Chile*
[12]*Vatican Observatory, Vatican City State, I-00120 Castello, Italy*
[13]*Departamento de Astronomía, Universidad de Concepción, Casilla 160-C, Concepción, Chile*

Accepted 2022 November 8. Received 2022 October 12; in original form 2022 January 21

ABSTRACT

We use data from the 17th data release of the Apache Point Observatory Galactic Evolution Experiment (APOGEE 2) to contrast the chemical composition of the recently discovered Gaia Enceladus/Sausage system (GE/S) to those of 10 Milky Way (MW) dwarf satellite galaxies: LMC, SMC, Boötes I, Carina, Draco, Fornax, Sagittarius, Sculptor, Sextans, and Ursa Minor. Our main focus is on the distributions of the stellar populations of those systems in the [Mg/Fe]–[Fe/H] and [Mg/Mn]–[Al/Fe] planes, which are commonly employed in the literature for chemical diagnosis and where dwarf galaxies can be distinguished from *in situ* populations. We show that, unlike MW satellites, a GE/S sample defined purely on the basis of orbital parameters falls almost entirely within the locus of 'accreted' stellar populations in chemical space, which is likely caused by an early quenching of star formation in GE/S. Due to a more protracted history of star formation, stars in the metal-rich end of the MW satellite populations are characterized by lower [Mg/Mn] than those of their GE/S counterparts. The chemical compositions of GE/S stars are consistent with a higher early star formation rate (SFR) than MW satellites of comparable and even higher mass, suggesting that star formation in the early universe was strongly influenced by other parameters in addition to mass. We find that the direction of the metallicity gradient in the [Mg/Mn]–[Al/Fe] plane of dwarf galaxies is an indicator of the early SFR of the system.

Key words: galaxies: dwarf – galaxies: Local Group – galaxies: abundances – galaxies: Magellanic Clouds.

1 INTRODUCTION

Our current understanding of galaxy formation is immersed in the framework of the Lambda cold dark matter (ΛCDM) model. In this model, galaxies are an ensemble of stars, gas, and dust bound by massive dark matter haloes, built largely by the merging of smaller systems (e.g. White & Rees 1978; Blumenthal et al. 1984; Frenk & White 2012). In this context, the Milky Way (MW) is of great importance, as the galaxy for which we can obtain the most detailed information. Naturally, one should expect that our knowledge of the MW should be used to constrain galaxy formation theory. While most of the stellar mass in the MW is contained in its bar and both thin and thick discs (Morris & Serabyn 1996; Barbuy, Chiappini & Gerhard 2018; Nataf 2017; Rich 2013; Beraldo e Silva et al. 2021), these structures are enveloped by a large stellar halo that contains about 1.3×10^9 $M_\odot$ in the form of stars (Mackereth & Bovy 2020).

Galaxy mergers were very common in the early universe. Local evidence of the merging activity of the MW has been accumulating over the years, with the identification of the remnants of multiple accretion events, starting with the discovery of the Sagittarius dwarf spheroidal (Sgr dSph) by Ibata, Gilmore & Irwin (1994). In addition, various stellar streams have been identified as remnants of past accretion events (e.g. Belokurov et al. 2006). Due to the stellar halo's

★ E-mail: r.p.schiavon@ljmu.ac.uk

long dynamical time-scale, such relatively recent accretion events can be identified in the form of spatial substructure. However, discerning the remnants of earlier accretion requires additional information, in the form of, e.g. kinematics, chemical compositions, and ages (e.g. Nissen & Schuster 2010, 2011; Schuster et al. 2012; Hayes et al. 2018)

With the advent of large spectroscopic surveys, we entered the golden age of Galactic archaeology. The information acquired by past, ongoing, and future surveys such as RAVE, (Steinmetz et al. 2006), SEGUE (Yanny et al. 2009), LAMOST (Cui et al. 2012), GALAH (De Silva et al. 2015), *Gaia* mission (Gaia Collaboration et al. 2016), WEAVE (Dalton 2016), APOGEE (Majewski et al. 2017), H3 (Conroy et al. 2019), MOONS (Cirasuolo et al. 2011; Gonzalez et al. 2020), 4MOST (de Jong et al. 2019) is very quickly advancing our understanding of the history of the MW. Chemical compositions and orbital information is becoming available for millions of stars in the MW and its Local Group companions. In addition, with the launching of the *Gaia* satellite (Gaia Collaboration et al. 2016), detailed phase space information has become available, enabling the identification of further substructures in the stellar halo of the Galaxy, associated with various accretion events, including Gaia-Enceladus/Sausage (GE/S), a massive dwarf galaxy accreted to the MW about ∼10 Gyr ago (Belokurov et al. 2018; Haywood et al. 2018; Helmi et al. 2018; Mackereth et al. 2019), as well as Heracles (Horta et al. 2021a), and various other substructures (e.g. Koppelman et al. 2019; Belokurov et al. 2018; Kruijssen et al. 2020; Naidu et al. 2020; Horta et al. 2022a).

Hawkins et al. (2015) and Das, Hawkins & Jofré (2020) have recently proposed that a combination of the abundances of Mn, Mg, Al, and Fe can be used to chemically discriminate accreted populations from their counterparts formed *in situ*. However, Horta et al. (2021a) used chemical evolution models to show that the region occupied by accreted populations in the [Mg/Mn] versus [Al/Fe] plane has a non-negligible presence of stars formed *in situ*.

It is difficult to disentangle metal-poor *in situ* populations from their accreted counterparts based on purely kinematic or orbital criteria. To minimize inter-sample contamination, one has to often resort to additional criteria based on chemical compositions, introducing sample biases that prevent a clean analysis of the chemical compositions of accreted and *in situ* populations. That difficulty can be overcome by resorting to data from external systems, on the assumption that the chemistry of their stellar populations is dominated by intrinsic evolutionary effects.

In this paper, we contrast the distribution of stars from GE/S system in key chemical composition planes with those of dwarf satellites of the MW. The latter include the Sagittarius dSph, which is currently in the process of being engulfed by the MW, as well as gas rich, irregular dwarf galaxies, such as the Large and Small Magellanic clouds (LMC & SMC); the gas-deficient, classical dwarf spheroidal galaxies (dSph), Carina, Draco, Fornax, Sculptor, Sextans, and Ursa-Minor; and the ultra-faint dwarf spheroidal galaxy, Boötes I. Our goal is to make inferences regarding the history of star formation and chemical enrichment of GE/S by contrasting it with MW satellites. We note that Hasselquist et al. (2021) have performed a similar comparative analysis of GE/S and massive satellites of the MW. In this paper, we extend the analysis to lower mass satellites, with a focus on the distribution of dwarf galaxy stellar populations on the [Mg/Mn]–[Al/Fe] plane and how it can be used to constrain the history of star formation of those systems. In addition, we examine the behaviour of chemical evolution models calculated for a range of relevant input parameters on that same chemical plane.

This paper is organized as follows. Section 2 presents the data and sample adopted. In Section 3, we present an examination of the distribution of the stellar populations of the various systems in key chemical planes. In Section 4, we contrast the chemical composition characteristics of GE/S with those of MW satellites of various masses, using chemical evolution models to guide the discussion. Our conclusions are presented in Section 5.

2 DATA AND SAMPLE

2.1 APOGEE DR17

The second-generation Apache Point Observatory Galactic Evolution Experiment (APOGEE-2; Majewski et al. 2017) is part of the Sloan Digital Sky Survey IV (Blanton et al. 2017). APOGEE-2 surveys the stellar populations of the MW with high-resolution ($R \sim 22\,500$), high S/N, spectroscopy in the *H*-band spectral region ($\lambda \sim 1.51$–1.70 μm), using two twin multi-fibre spectrographs (Wilson et al. 2019). Less hampered by interstellar dust than optical surveys its observations cover both Northern and Southern hemispheres, based primarily on the 2.5-m Sloan Foundation telescope (Gunn et al. 2006) at Apache Point Observatory and the 2.5-m Iréné du Pont telescope (Bowen & Vaughan 1973) at Las Campanas Observatory.

The data employed in this paper consist of chemical compositions, stellar parameters, and integrals of motion obtained from the 17th data release (DR17; Abdurro'uf et al. 2021; Holtzman et al. in preparation) of SDSS-IV/APOGEE-2. Chemical compositions and stellar parameters were generated by the APOGEE Stellar Parameter and Chemical Abundance Pipeline (ASPCAP; García Pérez et al. 2016), whereas the integrals of motion result from application of the `GALPY` package (Bovy 2015; Mackereth & Bovy 2018) to 6D phase space information resulting from combination of *Gaia* eDR3 proper motions (Gaia Collaboration et al. 2021), APOGEE-2 DR17 radial velocities (Nidever et al. 2015; Holtzman et al. in preparation), and `astroNN` machine learning-based distances (Leung & Bovy 2019). Calculations were performed adopting a McMillan (2017) potential for the Milky Way.

2.2 SELECTION CRITERIA

Our goal is to examine the chemical compositions of stars belonging to 10 dwarf satellites of the MW, namely LMC, SMC, Boötes I, Carina, Draco, Fornax, Sculptor, Sagittarius, Sextans, and Ursa Minor, contrasting their distributions in chemical diagnostic planes with those of the accreted system GE/S and the MW high- and low-α discs. The APOGEE-2 DR17 catalogue contains data for 733 901 stars, selected according to criteria extensively discussed by Zasowski et al. (2013, 2017) and Santana et al. (2021). Before selecting stars belonging to the above systems, we must apply a number of criteria to certify the quality of the data for our analysis. We first cleaned the sample from stars with unreliable parameters by removing all stars with STARFLAG or ASPCAPFLAG = **BAD** (see definitions in Holtzman et al. 2015). We then limit the data to red giant stars with S/N > 50, stellar effective temperatures ($T_{\rm eff}$) between 3750 and 5500 K, and surface gravity ($\log(g)$) < 3.0.

Next, we removed from the sample a total of 7562 stars that are deemed to be members of globular clusters, as listed in the Value Added Catalogue by Schiavon et al. (2022). Application of the above filters left us with a sample of 300 389 stars. The data for the objects of interest were extracted from this surviving catalogue according to the criteria described in the following sub-sections. The final sample sizes for each system are given in Table 1.

Table 1. Total sample selection.

Stellar structures	No. of stars in sample
Discs	193 220
LMC	4610
SMC	1660
Sgr	291
Boötes I	3
Carina	35
Draco	31
Fornax	140
Sculptor	85
Sextans	18
Ursa Minor	25
GE/S	1952

Table 2. MC sample selection.

LMC	SMC
α, δ : (80.893 860, −69.756 126)	α, δ : (13.186 67, −72.8286)
$d_{\rm proj} \leqq 12$	$d_{\rm proj} \leqq 8$
RV $\geqq 125$	RV $\geqq 100$
$2.7 \leqq \alpha$PM $\geqq 1$	$2.0 \leqq \alpha$PM $\geqq 0$
$2 \leqq \delta$PM $\geqq -1.2$	$-0.5 \leqq \delta$PM $\geqq -2.0$
$J - K \geqq 0.5$	J-K $\geqq 0.5$
$12.35 <$ H < 14.6	$12.9 <$ H < 14.7

Note. The table summaries the sky positions (α, δ), projected distance on the sky ($d_{\rm proj}$), *Gaia* proper motions (PM), radial velocities (RV), and magnitudes (H) for the LMC and SMC.

2.2.1 *Magellanic Clouds*

Our sample selection for the LMC and SMC members mimics that of Nidever et al. (2020) and is summarized in Table 2. We focus on the bright and faint red giant branch (RGB) stellar populations in the MCs (see their figs 3 and 5). In this way we expect to restrict our sample to stars in approximately the same evolutionary stage as those in the MW and other satellites.

2.2.2 *Sgr dSph*

Our sample for the Sgr dSph stars comes from the study by Hasselquist et al. (2017) and was selected by the methods described in Majewski et al. (2013). Further sampling of Sgr core and stream members are covered extensively in Hasselquist et al. (2019) and Hayes et al. (2020).[1] Table 3 summaries the selection criteria.

2.2.3 *Dwarf spheroidal galaxies*

APOGEE-2 has targeted a number of dwarf spheroidal galaxies. The field placement and target selection criteria adopted are described by Zasowski et al. (2017) and Santana et al. (2021). To identify dwarf spheroidal members, we first selected all stars observed within the fields of each dwarf galaxy and filtered out foreground contaminants on the basis of radial velocity and surface gravity. Stars considered members are giants ($\log g < 3.0$) whose heliocentric radial velocities differ from the central values for each galaxy by less than twice its velocity dispersion. By proceeding in this way, we prioritize sample purity over completeness. Radial velocities and velocity dispersions of the sample dSph galaxies are taken from table 1 from McConnachie & Venn (2020) and table 4 from McConnachie (2012)[2] with the exception of Boötes I, for which values were taken from Martin et al. (2007).

Table 3. Sgr sample selection.

Sagittarius dSph galaxy
α, δ : (284, −30)
$90 <$ RV < 220 km s^{-1}
$d > 5$ kpc
$J - K_0 > 0.8$
S/N > 70
$3550 < T_{\rm eff} < 4200$ K
$\log g < 4$

Note. The table summaries the sky positions (α, δ), radial velocities (RV), surface gravity ($\log g$), effective temperature ($T_{\rm eff}$), and signal-to-noise (S/N) selection criteria for the Sagittarius dSph galaxy core and tail.

Table 4. Properties of dSph Galaxies in the sample, including ID, stellar mass, velocity dispersion, radial velocity, and original references.

Galaxy	$M_\star$ (10^6M$_\odot$)	RV (km s^{-1})	σ (km s^{-1})	References
Boötes I	0.029	99.9 ± 2.4	$6.5^{+2.1}_{-1.3}$	(1)
Carina	0.38	222.9 ± 0.1	6.6 ± 1.2	(2)(6)(7)
Draco	0.29	−291 ± 0.1	9.1 ± 1.2	(2)(3)(4)
Fornax	20	55.3 ± 0.1	11.7 ± 0.9	(2)(6)(7)(9)
Sculptor	2.3	111.4 ± 0.12	9.2 ± 1.4	(2)(6)(7)(8)
Sextans	0.44	224.2 ± 0.1	7.9 ± 1.3	(2)(6)(7)
Ursa Minor	0.29	−246.9 ± 0.1	9.5 ± 1.2	(2)(4)(5)

References. (1) Martin et al. (2007), (2) Grcevich & Putman (2009), (3) Walker et al. (2007), (4) Wilkinson et al. (2004), (5) Walker et al. (2009b), (6) Walker, Mateo & Olszewski (2009a), (7) Walker, Mateo & Olszewski (2008), (8) Carignan et al. (1998), (9) Bouchard, Carignan & Staveley-Smith (2006). *Note*. All data from compilation by McConnachie (2012).

2.2.4 *Gaia-Enceladus/Sausage*

Stars from the accreted system GE/S are distributed throughout the MW and can be discriminated through a range of chemical, kinematical and/or orbital selection criteria. In order to obtain a GE/S sample devoid of chemical composition biases, we base our selection purely on integral of motion (IoM) measurements.

After removal from the sample of all stars associated to the MW satellites, the stellar populations of the accreted system GE/S are selected on the basis of their position in the energy versus angular momentum (E–L_z) plane.

A star is considered a member of the Gaia-Enceladus system if its energy and angular momentum fall within the following intervals:

(i) $-1.6 < E/10^5 < -1.3$ km^2 s^{-2};
(ii) $-0.4 < L_z/10^3 < 0.3$ kpc km s^{-1}.

This region of E–L_z is shown in Fig. 1. The above selection criteria mimic those adopted in previous work (e.g. Koppelman et al. 2019; Massari, Koppelman & Helmi 2019; Feuillet et al. 2021; Horta et al. 2021a). They are designed to take advantage of the overdensity in the E–L_Z plane around $L_Z \sim 0$ and at relatively high energy, which is easily identifiable in Fig. 1. We deliberately adopted a

[1] http://vizier.u-strasbg.fr/viz-bin/VizieR?-source = J/ApJ/889/63.

[2] http://www.astro.uvic.ca/~alan/Nearby_Dwarf_Database.html.

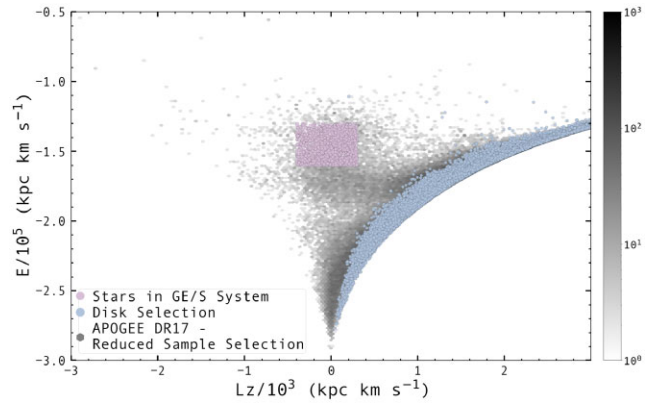

Figure 1. Selecting GE/S candidates in IoM in the plane of APOGEE DR17 stars, the number density is represented by the grey-scale colour bar and does not include the following stellar populations; thin-thick disc selection ($L_Z > 0$, eccentricity < 0.3), globular clusters (VAC by Schiavon et al. 2022, submitted), the Large and Small Magellanic clouds, Sagittarius dSph and low-mass dSph galaxies. The GE/S stars in this selection (pink thistle circles) are within $-1.6 < E/10^5 < -1.3$ km^2 s^{-2} and $-0.4 < L_z/10^3 < 0.3$ kpc km s^{-1}. The selection criteria of disc stars (light steel blue circles) in this analysis have been placed on top of the plane for reference.

relatively high lower energy limit for our GE/S selection with an eye towards minimizing disc contamination. Yet because we imposed no chemical composition cuts, we expect a small contamination of our GE/S sample by disc stars; see the discussion in Section 3.1. This contamination by disc stars is further enhanced by the existence of 'Splash' stars, which are early disc stars whose orbits were perturbed by the collision with GE/S (Belokurov et al. 2020). For a discussion of the impact of selection criteria on the chemical properties of GE/S, see Horta et al. (2022b).

2.2.5 Thin and thick disc

The stellar populations of the the MW disc are selected using orbital parameters in IoM, focusing on stars with circular, prograde orbits. We thus retain disc stars with the following criteria:

(i) $L_z > 0$;
(ii) eccentricity < 0.3;
(iii) S/N > 70.

The eccentricity cut employed is used to select stellar populations with disc orbits. The adopted eccentricity threshold is arbitrary. Placing the cut at, e.g. eccentricity < 0.2 or < 0.4 would cause no impact on our analysis. The detailed choice is not critical because the disc population is used solely as a reference for comparison with the dwarf satellite data.

3 CHEMICAL PROPERTIES

In the next two sections, we analyse the chemical properties of the dwarf galaxies and GE/S members alongside the MW discs in the chemical planes of Mg, Mn, Al, and [Fe/H].

3.1 Magnesium

Magnesium is an α-element synthesized during carbon burning in massive stars, and injected into the interstellar medium during Type II supernovae (SNe II) explosions (Kobayashi et al. 2006; Woosley & Weaver 1995). The distribution of the stellar populations on the α–Fe plane provides important clues on the star formation history and IMF of the system (e.g. Matteucci & Greggio 1986; Wheeler, Sneden & Truran 1989; McWilliam 1997).

In Fig. 2, the distributions of the stellar populations in the dwarf galaxies and GE/S stars are shown in the chemical plane of [Fe/H]–[Mg/Fe] across 11 panels, each displayed alongside the stellar populations of the low- and high-α discs of the MW, whose chemical compositions range roughly within $\sim -1.2 <$ [Fe/H] $< +0.65$ and $-0.2 <$ [Mg/Fe] $< +0.4$. These numbers are in good agreement with independent studies based on abundance analysis of high-resolution optical spectra, such as those by Aguado et al. (2021), Matsuno et al. (2021), and Carrillo et al. (2022).

We start by pointing out that, for the reasons discussed in Section 2.2, our GE/S sample contains a small, yet non-negligible, contamination by *in situ* stars, which can be easily spotted as they fall on the loci defined by the low- and high-α discs. It is fair to assume that the metal-rich stars in our GE/S sample that overlap with the high- and low-α disc sequences are contaminants because, on one hand, their chemical properties associate them strongly with the disc, and moreover it has been argued by Mackereth et al. (2018) and Mason et al. (in preparation) that low-mass galaxies do not host a bimodal α distribution. It is also likely that our sample may be contaminated on the metal-poor end, as *in situ* and accreted populations overlap on the [Mg/Fe]–[Fe/H] plane at low metallicity, (e.g. Horta et al. 2020). However, the disc sequence becomes very thinly populated at [Fe/H] $\lesssim -1.2$, and moreover our selection criteria prioritizing high-energy stars also helps minimizing disc contaminations. Thus, unless otherwise stated, our discussion henceforth ignores metal-rich contaminants overlapping with the high- and low-α disc sequences on both chemical planes under study.

The latter are characterized by predominantly low [Fe/H] and lower [Mg/Fe] than high-α disc stars at [Fe/H] $\gtrsim -1$, and overall decreasing with increasing metallicity. At the metal-poor end ([Fe/H] $\lesssim -1.8$), GE/S stars reach [Mg/Fe] values comparable or even slightly higher than those of the high-α disc, whereas at the metal-rich end ([Fe/H] ~ -0.6), GE/S stars have slightly lower [Mg/Fe] than that of low-α disc stars of same metallicity. The slope of the [Mg/Fe]–[Fe/H] relation undergoes a slight change, forming the so-called 'α-knee' at [Fe/H] ~ -1.2 (see also Mackereth et al. 2019; Horta et al. 2021a), which indicates the increased contribution of SN Ia to the chemical enrichment of the interstellar medium.

By and large, the locus occupied by GE/S stars in the Mg–Fe plane is somewhat similar to that where stars from the massive MW satellites LMC, SMC, and Sgr dSph are located (see also Hasselquist et al. 2021). The distributions, however, differ in important details. All three of the massive satellites show, at a given [Fe/H], a positive change in the slope of the [Mg/Fe]–[Fe/H] relation, whereby [Mg/Fe] starts increasing with increasing metallicity. This is likely associated with the occurrence of a burst of star formation in those systems, which causes an increase in the contribution of SNII to the chemical enrichment of the interstellar medium, resulting in a jump in [Mg/Fe] for increasing [Fe/H] (for a discussion, see Mason et al. in preparation). Because star formation in GE/S was quenched at the time of accretion, no similar change in slope can be seen in its stellar populations.

In contrast, for most low-mass dwarf spheroidal galaxies (except for Fornax), [Mg/Fe] decreases monotonically with increasing [Fe/H]. The slope of the relation is steeper than that of GE/S and the

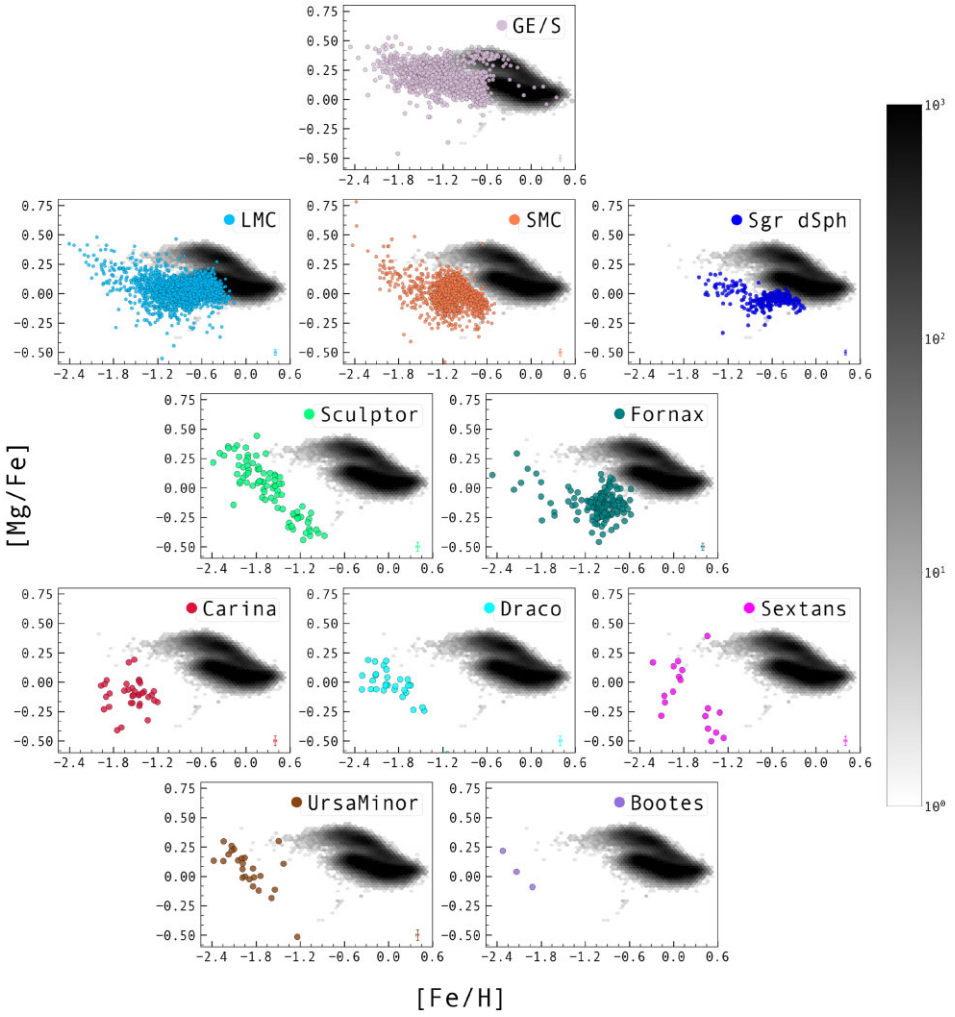

Figure 2. Stellar populations of the dwarf galaxies and GE/S in the plane of MW disc (marginal density 2D hexagonal binning – the greyscale of each hexbin denotes the number of points) in the chemical plane of [Mg/Fe] versus [Fe/H]. From top to bottom; the selected GE/S stellar population (thistle) as shown in Fig. 1, LMC (light blue), SMC (coral), Sgr dSph (blue), Sculptor (green), Fornax (teal), Carina (crimson), Draco (cyan), Sextans (fuchsia), Ursa Minor (brown), and Boötes I (purple).

more massive satellites, and the mean [Mg/Fe] is substantially lower in low-mass satellites. At [Fe/H] ~ -1.2 the stellar populations of low-mass satellites are lower in [Mg/Fe] by $\sim$0.2–0.4 dex than those from their massive counterparts.

The absence of a clear 'knee' in the α–Fe plane of low-mass satellites is likely due to it being located in those systems at metallicities that are lower than the values spanned by our sample. Indeed, previous studies of stars in Draco, Sextans and Ursa Minor (Shetrone et al. 2003), Sculptor (Hill et al. 2019), and Sextans (Theler et al. 2020) suggest the presence of a 'knee' at [Fe/H] ~ -2. Based on a compilation of chemical compositions from various works (Cohen & Huang 2009, 2010; Starkenburg et al. 2013), Hendricks et al. (2014) quote $[Fe/H]_{knee} \sim -1.9$ for Sculptor, Ursa Minor, and Fornax and $[Fe/H]_{knee} \lesssim -2.5$ for Draco and Carina (see also de Boer et al. 2014). The low-metallicity limit of our sample prohibits any statement on the existence of a change of slope for the latter two galaxies. As for the others, while our data do not rule out the presence of a change of slope in the Mg–Fe relation for Sculptor, Ursa Minor, and Fornax at [Fe/H] ~ -2, they cannot confirm it either, due to increased uncertainties and relatively small sample sizes in the low metallicity end.

The above result, taken together with the overall lower [Mg/Fe] of lower mass satellites, suggests that the contribution by SN Ia to the chemical enrichment of the interstellar medium of those satellites was more dominant than in their massive counterparts, possibly indicating a lower star formation rate (SFR) throughout their histories (e.g. Mason et al. in preparation). The one exception is Fornax, for which a sharp positive change of slope can be seen at [Fe/H] ~ -1.2, similar to the case of more massive satellites, suggesting also in the case of Fornax the occurrence of a burst of star formation in the recent past.

Most importantly for the goals of this study, when we contrast the position of GE/S in the Mg–Fe plane with those of dwarf satellites of the MW, we conclude that it has undergone an intense early history of star formation leading up to the build-up of a relatively metal-rich and α-enhanced stellar population, akin to those of the massive satellites of the MW. This is not surprising, considering current estimates for the original mass of the GE/S progenitor ($\sim 10^8$–$10^9 M_\odot$; e.g. Helmi et al. 2018; Belokurov et al. 2018; Mackereth et al. 2019; Deason, Belokurov & Sanders 2019; Mackereth & Bovy 2020; Feuillet et al. 2020).

3.2 Aluminium and manganese [Al, Mn]

It is well known that stellar population diagnosis is substantially improved by the consideration of the abundances of elements associated with distinct nucleosynthetic pathways. In that vein, it has been proposed by Hawkins et al. (2015) and Das et al. (2020) that the combination of the abundances of Fe, Mg, Mn, and Al can aid in the discrimination of accreted stellar populations in the Galactic halo. Manganese is an Fe-peak element generated in Type Ia supernovae (SN Ia) (Iwamoto et al. 1999; Hillebrandt & Niemeyer 2000; Weinberg et al. 2019). According to Hawkins et al. (2015), manganese is a more pure indicator of enrichment by SNe Ia than iron, which makes that element particularly useful for chemical diagnosis. Unlike the case of [Mg/Fe], [Mn/Fe] correlates positively with metallicity (Kobayashi, Leung & Nomoto 2020). This sharp distinction between the dependence of Mg and Mn on metallicity makes the ratio between these two elements a powerful discriminator between stellar populations with different chemical evolution histories.

Aluminium, in turn, is referred to as an odd-*Z* element. Although similarly to magnesium, Al is produced predominantly by SNe II (Buchmann et al. 1984; Prantzos & Diehl 1996), it can be contributed relevantly by a number of other nucleosynthetic sources. Aluminium primarily forms during H burning phases in the CNO, NeNa and MgAl cycles (Samland 1998; Guelin et al. 1995). A small amount of Al is also created in white dwarf binary collisions (Nofar, Shaviv & Starrfield 1991; Weiss & Truran 1990). Other sources of Al are observed from the winds of Wolf–Rayet (Limongi & Chieffi 2006) and AGB stars (Nomoto, Thielemann & Yokoi 1984). Furthermore, viable sources of ^{26}Al in the ISM are thought to originate from the accretion of hydrogen-rich gas in white dwarf binaries following novae explosions (Gehrz et al. 1998; Kamiński et al. 2018; Clayton 1984).

Das et al. (2020) used the SDSS-III/APOGEE DR14 sample (Abolfathi et al. 2018; Holtzman et al. 2018) to show that stars belonging to the GE/S system occupy a distinct locus in the [Al/Fe] versus [Mg/Mn] plane, characterized by low [Al/Fe] and high [Mg/Mn]. More recently, Horta et al. (2021a) used chemical evolution models to show that this particular locus of chemical space is actually the home of *chemically unevolved* stellar populations. In other words, any early stellar populations inhabit that region of chemical space, regardless of where they are formed. As chemical evolution proceeds, the elemental abundances of *in situ* populations move away from that locus of chemical space, whereas the star formation of early accreted systems is quenched, so that chemical compositions are frozen in their early, pre-accretion state.

4 STELLAR POPULATIONS: CHEMICALLY EVOLVED OR UNEVOLVED

In this section, we examine the distribution of GE/S stars and MW dwarf satellites in the [Al/Fe] versus [Mg/Mn] plane, in order to check whether the above scenario is supported by an entirely empirical examination of the data. For that purpose, we compare the distribution of GE/S stars in that plane with those of the low- and high-mass satellites of the MW.

4.1 The detailed chemistry of a kinematically selected GE/S

Our first goal is to check whether the locus of a GE/S sample selected purely on the basis of kinematics would be concentrated in the 'chemically unevolved' region of the [Mg/Mn]–[Al/Fe] space. We recall that, for this analysis to be meaningful, it is critical that the selection of the stars from all systems is entirely free of any chemical composition criterion (for details, see Section 2.2.4).

Inspection of Fig. 3 shows that the majority of GE/S stars selected purely on the basis of orbital parameters fall within the 'chemically unevolved' locus of the [Mg/Mn]–[Al/Fe] space where 82 per cent of GE/S stars are located. It is important, however, to keep in mind that this line is arbitrary so that it is possible that some stars in the 'evolved' region actually belong to GE/S. There is a small amount of contamination by high-α disc stars, spreading towards the high [Al/Fe] and high [Mg/Mn] (upper right) locus of the chemical space. In contrast to the case of [Mg/Fe] abundance ratios, all the dwarf galaxies and GE/S are characterized by similarly low [Al/Fe]. In fact, at [Fe/H] $\lesssim -1.0$, the bulk [Al/Fe] abundances in the dwarf galaxies are lower than those in the low- and high-α discs.

Our GE/S sample stars fall squarely within the 'chemically unevolved' region of the plot, which we interpret as indicating an early quenching of star formation taking place during the merger of that galaxy with the MW (see the discussion in Feuillet et al. 2021). This result confirms our interpretation of the distribution of the stellar populations in the [Mg/Mn]–[Al/Fe] plane, as well as the chemical evolution calculations presented in Horta et al. (2021b).

4.2 GE/S versus dwarf satellites

We next compare the distribution of GE/S stars in the [Al/Fe] versus [Mg/Mn] plane with those of the massive MW satellites (MCs and Sgr dSph). In contrast to the case of GE/S, a substantial fraction of the stars in the MCs and the Sgr dSph lie outside that locus. This is not surprising, as these massive satellites continued forming stars long after star formation in GE/S had ceased. The chemically evolved, more metal-rich, stars in those massive satellites spread towards the low [Mg/Mn] region of the plane, at approximately constant [Al/Fe]. It is also worth noticing that those among the stars belonging to the massive satellite that do inhabit the 'chemically unevolved' locus of the plot are located towards a substantially lower mean [Mg/Mn] than the stars from GE/S. While the GE/S stars within the 'chemically unevolved' region have mean [Mg/Mn] ~ 0.50, those in the MCs and Sgr dSph have mean values between $\sim$0.35 and 0.25 dex lower. We speculate whether this difference is due to a selection effect caused by the fact that the massive satellites samples may be biased towards the high metallicity end of the MDF.

Differences between the loci occupied by GE/S and lower mass satellites are even more pronounced, particularly for Draco, Carina, Sextans, and Ursa Minor, whose sample stars are predominantly located outside the 'chemically unevolved' region. While this difference may partly reflect selection biases, it is qualitatively consistent with these lower mass satellites having undergone an evolutionary history characterized by a low, yet more prolonged, SFR than those of GE/S and the massive MW satellites, which would naturally lead to a stronger contribution to enrichment by SN Ia and a consequently lower mean [Mg/Mn]. This is further discussed in Section 4.5.

4.3 Comparison with chemical evolution models

In Fig. 4, we build on the diagnostic [Al/Fe]–[Mg/Mn] plane with the addition of two chemical evolution models calculated using the FLEXCE code from Andrews et al. (2017). The orange line shows the evolution of a model made to match the properties of the stellar populations of the solar neighbourhood, representing an *in situ* population, and the yellow model line shows a chemical evolution

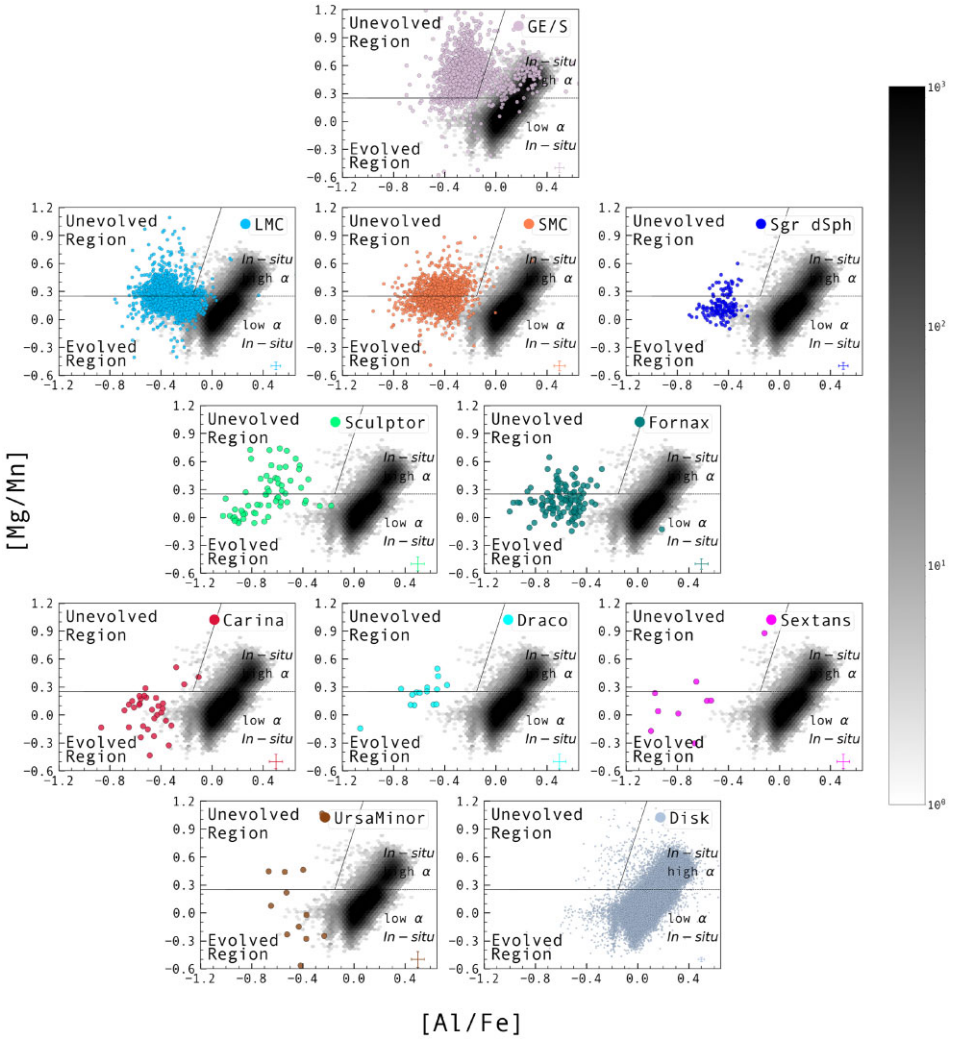

Figure 3. Diagnostic plot [Al/Fe]–[Mg/Mn]. Stellar populations of the dwarf galaxies and GE/S in the plane of MW disc (marginal density 2D hexagonal binning – the greyscale of each hexbin denotes the number of points). From the top to bottom: the selected GE/S stellar population (thistle) as shown in Fig. 1, LMC (light blue), SMC (coral), Sgr dSph (blue), Sculptor (green), Fornax (teal), Carina (crimson), Draco (cyan), Sextans (fuchsia), Ursa Minor (brown), and the disc selection (steel blue), as shown in Fig. 1. Black lines separate *in situ* high-α, *in situ* low-α stars, and the unevolved region.

model built to match the chemical properties of GE/S, characterizing the chemical evolution of a relatively massive satellite galaxy. The parameters adopted for the chemical evolution models are shown in Table 5. The *in situ* MW model is outlined in Horta et al. (2020). The model for GE/S was built to match the distribution of the data on the Si–Fe plane. For details on the model parameters, see tables 3 and 4 of Hasselquist et al. (2021). The models evolve for approximately 13 Gyr: the filled circles on the models mark the evolutionary times at 0.3, 1, and 5 Gyr. The black cross marks the position at which the iron abundance reaches [Fe/H] = –1. The star formation efficiencies in the two models differ by an order of magnitude, at 1.5 Gyr^{-1} in the *in situ* case (Horta et al. 2021b) and 0.14 Gyr^{-1} for the best-fitting GE/S model (Hasselquist et al. 2021). As a result, the solar neighbourhood model reaches [Fe/H] = –1 a mere 0.12 Gyr after the beginning of the evolution, whereas the GE/S model takes $\sim$ 1.18 Gyr to reach the same metallicity. The models provide a qualitatively good description of the data for the *in situ*, accreted, and satellite stellar populations on the [Mg/Mn] versus [Al/Fe] plane. These model calculations are an important tool for the interpretation of the data. In both cases, the early chemical enrichment drives the evolution towards the right due to the contribution by SNe II/core collapse SNe because [Mg/Mn] remains approximately constant, while [Al/Fe] grows due to the metallicity dependence of Al yields. By the same token, downward/left evolution on this plane reflects the increased contribution by SN Ia.

The data for the various accreted/satellite stellar populations in Fig. 4 are colour-coded by metallicity. One can immediately notice a difference between GE/S and all the MW satellites, which have lower [Al/Fe] on average than GE/S. Indeed, the model is a good match to GE/S, by construction, while failing to reproduce the main locus of satellites, which is particularly noteworthy in [Al/Fe]. Given the clear dependence of the value of [Al/Fe] on star formation efficiency indicated by the models, this difference suggests that GE/S formed stars more vigorously early in its history than the MW satellites. In Section 4.5, we discuss the behaviour of chemical evolution models on this plane in more detail.

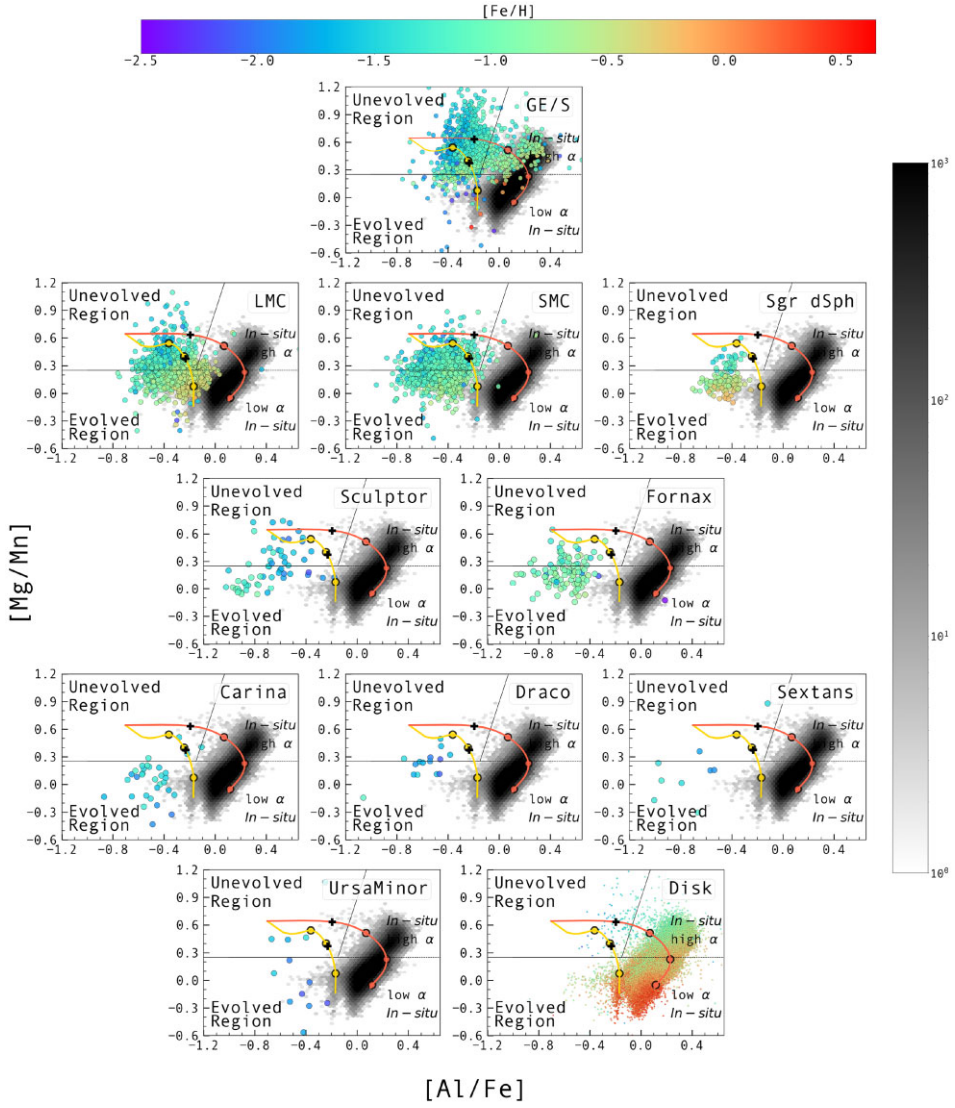

Figure 4. Diagnostic plot [Al/Fe]–[Mg/Mn], colour-coded by metallicity. The MW Chemical Evolution Model (orange) and Dwarf Chemical Evolution Model (yellow) in the [Mg/Mn] versus [Al/Fe] abundance plane. Coloured circles mark the evolutionary times at 0.3, 1.0, and 5.0 Gyr. Black cross is the position at which the models reach [Fe/H] $= \sim -1$: $t = 0.1$ Gyr for the MW chemical evolution model and $t = 1.2$ Gyr for the dwarf chemical evolution model. From the top to bottom: GE/S, LMC, SMC, Sgr dSph, Sculptor, Fornax, Carina, Draco, Sextans, Ursa Minor, and the disc. Black lines separate *in situ* high-α, *in situ* low-α stars, and the unevolved region.

Table 5. Summary of parameters used in the chemical evolution models.

Model Parameters	MW	GE/S	LMC-like	Sgr dSph-like	Sculptor-like
Initial gas mass	2×10^{10} M$_\odot$	3×10^{9} M$_\odot$	3×10^{9} M$_\odot$	3×10^{9} M$_\odot$	3×10^{9} M$_\odot$
Inflow mass scale	3.5×10^{11} M$_\odot$	6×10^{10} M$_\odot$	6×10^{10} M$_\odot$	6×10^{10} M$_\odot$	6×10^{10} M$_\odot$
Outflow mass loading factor	2.5	6	5.4	20	40
Star formation efficiency	1×10^{-9} yr^{-1}	1.5×10^{-10} yr^{-1}	1.25×10^{-11} yr^{-1}	2.5×10^{-11} yr^{-1}	1×10^{-11} yr^{-1}
Exponential inflow time-scale	6 Gyr	2.5 Gyr	2.5 Gyr	2.5 Gyr	2.5 Gyr

4.4 Metallicity gradients on the [Mg/Mn]–[Al/Fe] plane

We call attention to an important feature in the distribution of the data for different stellar populations in Fig. 4. As the points are colour-coded by metallicity, one can see that the colour gradient on the [Mg/Mn] versus [Al/Fe] plane, varies widely from galaxy to galaxy, with more metal-rich stars being distributed towards the lower right in more massive systems and towards the lower left in low-mass satellites. This suggests that GE/S and the MCs seem to have evolved more quickly in [Al/Fe] than all the other surviving satellites of the MW (this is true even after correction for contamination by *in situ* stars; see Section 4.4).

We quantified this effect by measuring the metallicity gradients of our sample galaxies in the [Mg/Mn]–[Al/Fe] plane as follows.

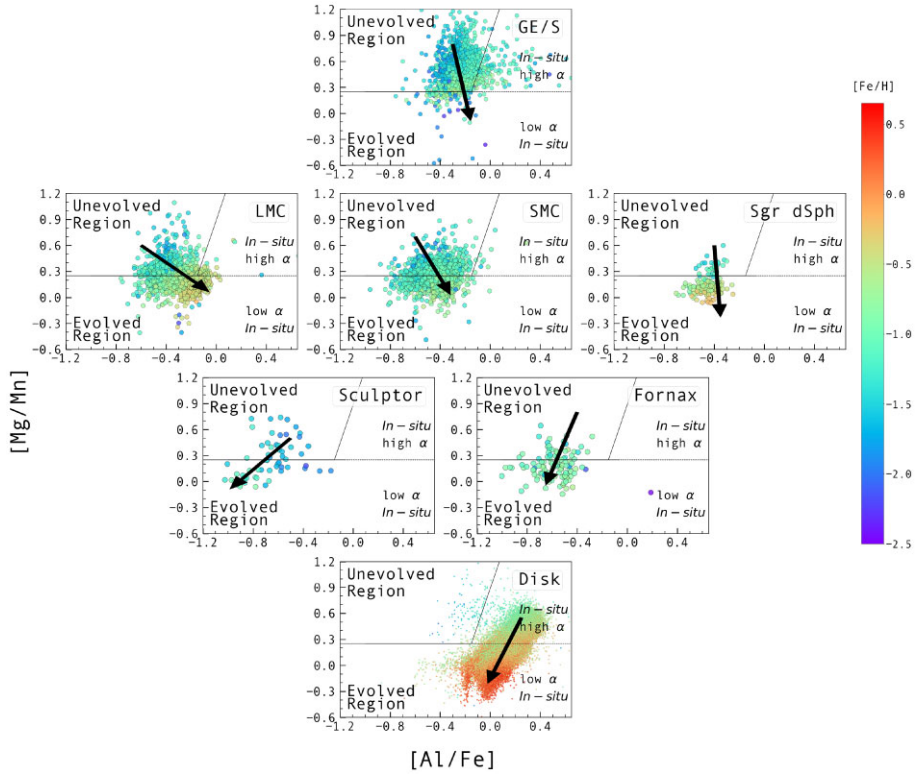

Figure 5. Diagnostic plot [Al/Fe]–[Mg/Mn], colour-coded by metallicity. From the top to bottom: GE/S stellar population (excluding the contaminating thick-disc/high-α stars), LMC, SMC, Sgr dSph, Sculptor, Fornax, and the disc selection as shown in figure 1. Black lines separate *in situ* high-α, *in situ* low-α stars, and the unevolved region. In each panel, the direction of the arrow represents the metallicity vector of the stellar population.

We first reduced the sample in two ways. For GE/S, we minimized contamination by *in situ* stars by selecting them in the Mg–Fe plane in the same way as Horta et al. (2021a, see their appendix). In addition, we reduced the overall sample to stars with the most reliable elemental abundances. The APOGEE/ASPCAP abundance measurements for Fe, Mg, and Al are quite reliable in the range of metallicities spanned by our data. However, the abundance of Mn relies on a few relatively weak lines, becoming more uncertain in the low-metallicity end. We examined the spectra of sample stars in a range of metallicities and S/N ratios and decided to restrict the sample to stars with [Fe/H] > -1.6 and, for those with [Fe/H] < -1.5, we only kept spectra with S/N > 70. As a result, the samples for Carina, Draco, Sextans, and Ursa Minor become too small and they are not included in this analysis. On the basis of this reduced sample, we fit linear relations to the data for each galaxy in the [Mg/Mn]–[Fe/H] and [Al/Fe]–[Fe/H] planes and derive the coefficients of the relations in the [Mg/Mn]–[Al/Fe] plane.

The result is displayed in Fig. 5, where arrows indicating the direction (but not the modulus) of the metallicity gradients are overlaid on the reduced samples described above. The arrows confirm the visual impression about the direction of chemical evolution on the diagnostic plane of Figs 3–5. In massive MW satellites, the arrow points towards the lower right, whereas in lower mass satellites and the MW disc, it points towards the lower left. Along the same lines, the direction of the metallicity gradient in the disc population points strongly towards the lower left of the chemical plane. That is also the case of the disc of the MW.

As indicated by the models in Fig. 4, the overall direction of the metallicity gradient vector in the [Mg/Mn]–[Al/Fe] plane seems to be dependent on the star formation history of the system, which in turn is associated with its mass. It is therefore instructive to examine the behaviour of stellar populations on this chemical plane on the basis of chemical evolution models sampling a wider range of input parameters. That is the topic of the next subsection.

4.5 Chemical evolution on the [Mg/Mn]–[Al/Fe] plane

In this Section we further examine the hypothesis that the metallicity gradient in the [Mg/Mn]–[Al/Fe] plane is sensitive to the SFR. For that purpose we calculated further chemical evolution models building on those presented in Fig. 4, based on FLEXCE (Andrews et al. 2017). The same yields and SNe Ia delay time distribution are adopted in all calculations. In order to produce a spectrum of models that replicate the behaviour of dwarfs of different masses in this chemical plane, we adopt a range of values for the star formation efficiency (SFE) and the wind mass-loading factor (η), which are, respectively, positively and negatively correlated with galaxy mass. For GE/S and MW, we adopt the same models as discussed in Section 4.3. Table 5 summarizes how these parameters differ between the models. They are chosen to cover, in a qualitative fashion, the range of properties characteristic of the dSph galaxies included in our sample. Specific parameters adopted are tuned to approximately match the properties of the MCs (MC-like), Sgr dSph (Sgr-like), and the lower mass galaxies (Sculptor-like).

The results are displayed in Fig. 6. The top panel shows evolutionary tracks on the [Mg/Mn]–[Al/Fe] plane, whereas the star formation histories are plotted in the bottom panel. As in Fig. 4, evolutionary times of 0.3, 1.0, and 5.0 Gyr are indicated for each model.

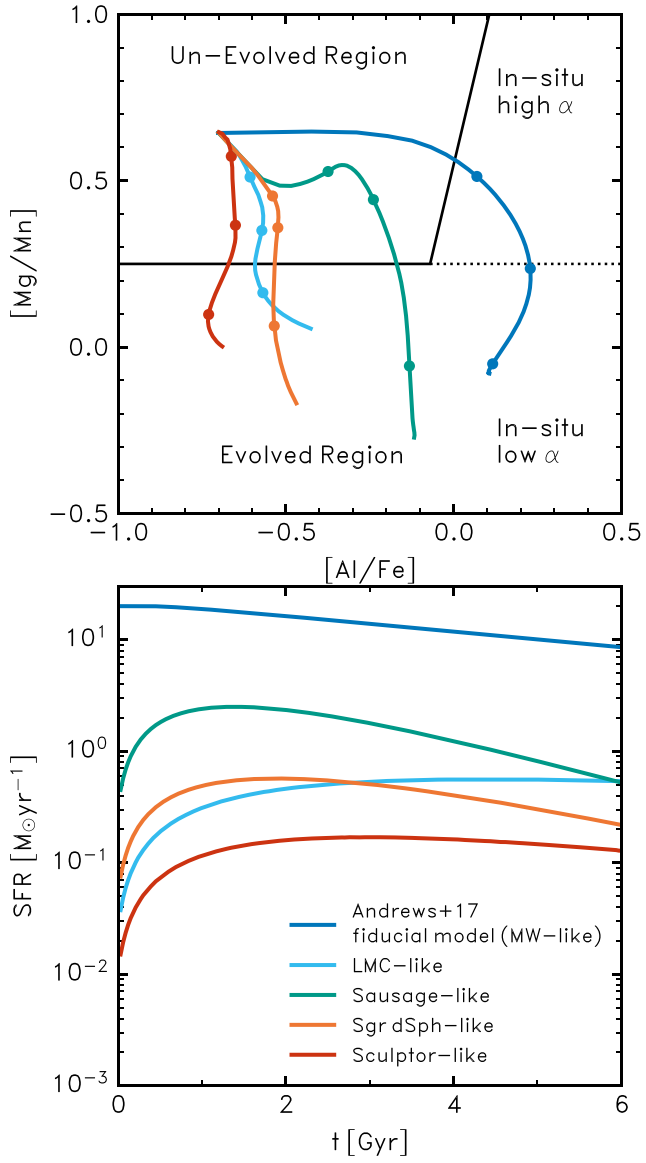

Figure 6. Chemical evolution and star formation histories for a series of one-zone open box models ran using the FLEXCE code. Top panel: tracks of [Mg/Mn](t) plotted as a function of [Al/Fe](t). Bottom panel: SFR as a function of time, SFR(t). The solid blue tracks illustrate the fiducial model of Andrews et al. (2017) as shown in Fig. 4. For the other models, for a fixed history of gas inflow, we vary the star formation efficiency and the wind mass loading factor (η) so as to qualitatively capture the behaviour of a selection of the Local Group dwarfs in our sample with varying stellar masses. Parameters adopted are listed in Table 5.

An examination of the behaviour of these various models is quite informative. We start by considering the fiducial MW model (Table 5), represented by the solid blue line. It is the one for which the SFR is by far the largest, exceeding those of the other models by at least an order of magnitude. On account of such a very high SFR, enrichment is initially entirely dominated by massive stars. Thus, the [Mg/Mn] ratio remains very high in the first few 100 Myr of evolution, whereas [Al/Fe] builds up very quickly. With the increasing contribution by SN Ia at $t \gtrsim 300$ Myr, [Mg/Mn] starts declining steadily. As the SFR declines further, so does the [Mg/Mn] ratio, and eventually the contribution by SN Ia becomes important enough that the [Al/Fe] ratio starts declining, after about 1 Gyr of evolution.

Table 6. Mean abundances and their dispersions of MW satellites in our sample.

System	⟨[Al/Fe]⟩	σ[Al/Fe]	⟨[Mg/Mn]⟩	σ[Mg/Mn]
GE/S	−0.21	0.17	0.50	0.20
GE/S (clean)	−0.23	0.14	0.51	0.20
SMC	−0.42	0.13	0.27	0.14
LMC	−0.31	0.12	0.23	0.13
Sgr	−0.46	0.08	0.14	0.10
Sculptor	−0.64	0.20	0.28	0.31
Fornax	−0.59	0.17	0.17	0.18

The remainder of this discussion contrasts the behaviour of various models within the first Gyr of cosmic evolution, where enrichment of the elements involved is dominated by CCSNe and SN Ia. In all of the dwarf-like models, the initial SFR is substantially lower than for the MW model. As a result, within the first few 100 Myr, the evolution in [Al/Fe] is slower while [Mg/Mn] is more strongly influenced by the SN Ia enrichment. Hence, with decreasing SFR the early evolutionary tracks switch from pointing straight to the right to instead pointing at increasing degrees towards the lower right, and finally towards the lower left. Indeed, as suggested by the discussion in the previous section, within the first Gyr of evolution, there is a clear correlation between the orientation of the track on the [Mg/Mn]–[Al/Fe] plane and the SFR.

This qualitative analysis can inform an interpretation of broad trends that one can promptly grasp from even a perfunctory evaluation of the data. For instance, it is easy to see from Figs 3 and 4 that the data for GE/S are shifted towards higher [Al/Fe] and [Mg/Mn] than those of the MCs, which, in turn, have higher values than the lower mass MW satellites. The numbers are summarized in Table 6. The mean values for [Mg/Mn] and [Al/Fe] are substantially larger in GE/S than in all the MW satellites which, according to our interpretation of the models, suggests a stronger SFR in the early stages of evolution, in agreement with the results by Hasselquist et al. (2019). The same conclusion can be drawn when comparing the massive MW satellites with their less massive counterparts, whose data suggest a slower rate of chemical evolution, associated with a weaker SFR.

Subsequent evolution, beyond ∼1 Gyr, seems to be dictated by the slope of the SFR. Models with strongly decreasing SFR (e.g. MW, Sausage-, and Sgr-like) tend to evolve more strongly towards lower [Mg/Mn] with more or less constant [Al/Fe], whereas those with more approximately constant SFR (e.g. Sculptor- and LMC-like) display a slight turn over of [Al/Fe] and slower decline in [Mg/Mn]. These trends ultimately reflect the balance between the contribution by CCSNe and SN Ia (and AGB stars in the case of Al) to the chemical enrichment of the interstellar medium (see Mason et al. in preparation, for a detailed discussion).

The contrast between the histories of star formation of GE/S and massive MW satellites, and in particular the LMC and SMC is interesting in light of the fact that the mass of GE/S, according to various studies, is of the order of a few to several times 10^8 $M_\odot$ (e.g. Lane, Bovy & Mackereth 2021; Deason et al. 2019; Mackereth et al. 2019), which is comparable to that of the SMC ($\sim 5 \times 10^8$ $M_\odot$) and smaller than that of the LMC ($\sim 1.5 \times 10^9$ $M_\odot$; McConnachie 2012). That galaxies with similar masses have undergone such vastly different histories of star formation indicates a physical variable other than mass is at play at regulating the

star formation histories of dwarf galaxies. Hasselquist et al. (2021) suggest it is the environment in which the dwarf galaxies formed and evolved. We tackle this problem from the point of view of numerical cosmological simulations in a forthcoming paper (Mason et al. in preparation).

5 CONCLUSIONS

We present a comparative study of the distribution in chemical diagnostic planes of the stellar populations of the GE/S system and those of satellites of the MW. Our main conclusions are the following:

(i) We investigate the location on the [Mg/Mn] versus [Al/Fe] plane of a GE/S sample defined purely on the basis of orbital properties. When selected in this way, GE/S stars lie almost entirely within the locus of that chemical plane deemed to contain 'accreted' populations by Das et al. (2020) and Hawkins et al. (2015). While this result validates previous use of that method for the identification of stellar populations formed *ex situ*, caution is recommended, since old populations formed *in situ* share the same locus, as shown by Horta et al. (2021a). We therefore propose adopting a 'chemically unevolved' nomenclature when referring to that particular locus of chemical space.

(ii) The stellar populations of the satellites of the MW are mostly divided between the chemically evolved and unevolved loci on this plane. The chemically evolved, more metal-rich stars are located towards the region of lower [Mg/Mn] and approximately constant, or slightly different, [Al/Fe].

(iii) The distribution of GE/S stars on the [Mg/Mn]–[Al/Fe] plane differs from those of MW satellites in an important respect. The chemical evolution of its stellar populations in this plane suggest a higher *early* SFR than MW satellites with comparable or even higher masses, as suggested by Hasselquist et al. (2019).

(iv) The direction of the metallicity vector on the [Mg/Mn]–[Al/Fe] plane is an indicator of the early SFR of a system. Higher mass galaxies and/or those undergoing high SFRs evolve more quickly in [Al/Fe] than in [Mg/Mn]. The existence of this trend is suggested by the APOGEE data on the stellar populations of the systems under study, and is boldly confirmed by the predictions of analytical chemical evolution models. The ensuing interpretation of our data on MW satellites in the light of such models leads to the conclusion that the early SFRs of these systems was strongly affected by parameters other than galaxy mass.

ACKNOWLEDGEMENTS

Funding for the Sloan Digital Sky Survey IV has been provided by the Alfred P. Sloan Foundation, the US Department of Energy Office of Science, and the Participating Institutions.

SDSS-IV acknowledges support and resources from the Center for High Performance Computing at the University of Utah. The SDSS website is www.sdss.org.

SDSS-IV is managed by the Astrophysical Research Consortium for the Participating Institutions of the SDSS Collaboration including the Brazilian Participation Group, the Carnegie Institution for Science, Carnegie Mellon University, Center for Astrophysics | Harvard & Smithsonian, the Chilean Participation Group, the French Participation Group, Instituto de Astrofísica de Canarias, The Johns Hopkins University, Kavli Institute for the Physics and Mathematics of the Universe (IPMU)/University of Tokyo, the Korean Participation Group, Lawrence Berkeley National Laboratory, Leibniz Institut für Astrophysik Potsdam (AIP), Max-Planck-Institut für Astronomie (MPIA Heidelberg), Max-Planck-Institut für Astrophysik (MPA Garching), Max-Planck-Institut für Extraterrestrische Physik (MPE), National Astronomical Observatories of China, New Mexico State University, New York University, University of Notre Dame, Observatário Nacional / MCTI, The Ohio State University, Pennsylvania State University, Shanghai Astronomical Observatory, United Kingdom Participation Group, Universidad Nacional Autónoma de México, University of Arizona, University of Colorado Boulder, University of Oxford, University of Portsmouth, University of Utah, University of Virginia, University of Washington, University of Wisconsin, Vanderbilt University, and Yale University.

This work has made use of data from the European Space Agency (ESA) mission *Gaia* (https://www.cosmos.esa.int/gaia), processed by the *Gaia* Data Processing and Analysis Consortium (DPAC; https://www.cosmos.esa.int/web/gaia/dpac/consortium). Funding for the DPAC has been provided by national institutions, in particular the institutions participating in the *Gaia* Multilateral Agreement.

Softwares: ASTROPY (Astropy Collaboration et al. 2013, 2018), SCIPY (Virtanen et al. 2020), NUMPY (Oliphant 2006; Harris et al. 2020), MATPLOTLIB (Hunter 2007), GALPY (Bovy 2015), TOPCAT (Taylor 2005), FLEXCE (Andrews et al. 2017).

DATA AVAILABILITY

This research was made possible with data from the SDSS-IV/APOGEE-2, 17th data release and *Gaia* eDR3, publicly available at https://www.sdss.org/dr17/irspec/spectro_data/ and https://gea.esac.esa.int/archive/, respectively.

REFERENCES

Abdurro'uf et al., 2021, ApJS, 259, 39
Abolfathi B. et al., 2018, ApJS, 235, 42
Aguado D. S. et al., 2021, ApJ, 908, L8
Andrews B. H., Weinberg D. H., Schönrich R., Johnson J. A., 2017, ApJ, 835, 224
Astropy Collaboration et al., 2013, A&A, 558, A33
Astropy Collaboration et al., 2018, AJ, 156, 123
Barbuy B., Chiappini C., Gerhard O., 2018, ARA&A, 56, 223
Belokurov V. et al., 2006, ApJ, 642, L137
Belokurov V., Erkal D., Evans N. W., Koposov S. E., Deason A. J., 2018, MNRAS, 478, 611
Belokurov V., Sanders J. L., Fattahi A., Smith M. C., Deason A. J., Evans N. W., Grand R. J., 2020, MNRAS, 494, 3880
Beraldo e Silva L., Debattista V. P., Nidever D., Amarante J. A. S., Garver B., 2021, MNRAS, 502, 260
Blanton M. R. et al., 2017, AJ, 154, 28
Blumenthal G. R., Faber S. M., Primack J. R., Rees M. J., 1984, Nature, 311, 517
Bouchard A., Carignan C., Staveley-Smith L., 2006, AJ, 131, 2913
Bovy J., 2015, ApJS, 216, 29
Bowen I. S., Vaughan A. H. J., 1973, Appl. Opt., 12, 1430
Buchmann L., Hilgemeier M., Krauss A., Redder A., Rolfs C., Trautvetter H. P., Donoghue T. R., 1984, Nucl. Phys. A, 415, 93
Carignan C., Beaulieu S., Côté S., Demers S., Mateo M., 1998, AJ, 116, 1690
Carrillo A., Hawkins K., Jofré P., de Brito Silva D., Das P., Lucey M., 2022, MNRAS, 513, 1557
Cirasuolo M., Afonso J., Bender R., Bonifacio P., Evans C., Kaper L., Oliva E., Vanzi L., 2011, The Messenger, 145, 11
Clayton D. D., 1984, ApJ, 280, 144
Cohen J. G., Huang W., 2009, ApJ, 701, 1053
Cohen J. G., Huang W., 2010, ApJ, 719, 931
Conroy C. et al., 2019, ApJ, 883, 107
Cui X.-Q. et al., 2012, Res. Astron. Astrophys., 12, 1197

Dalton G., 2016, in Skillen I., Balcells M., Trager S., eds, ASP Conf. Ser. Vol. 507, Multi-Object Spectroscopy in the Next Decade: Big Questions, Large Surveys, and Wide Fields. Astron. Soc. Pac., San Francisco, p. 97
Das P., Hawkins K., Jofré P., 2020, MNRAS, 493, 5195
de Boer T. J. L., Tolstoy E., Lemasle B., Saha A., Olszewski E. W., Mateo M., Irwin M. J., Battaglia G., 2014, A&A, 572, A10
de Jong R. S. et al., 2019, The Messenger, 175, 3
De Silva G. M. et al., 2015, MNRAS, 449, 2604
Deason A. J., Belokurov V., Sanders J. L., 2019, MNRAS, 490, 3426
Feuillet D. K., Feltzing S., Sahlholdt C. L., Casagrande L., 2020, MNRAS, 497, 109
Feuillet D. K., Sahlholdt C. L., Feltzing S., Casagrande L., 2021, MNRAS, 508, 1489
Frenk C. S., White S. D. M., 2012, Ann. Phys., 524, 507
Gaia Collaboration et al., 2016, A&A, 595, A1
Gaia Collaboration et al., 2021, A&A, 649, A1
García Pérez A. E. et al., 2016, AJ, 151, 144
Gehrz R. D., Truran J. W., Williams R. E., Starrfield S., 1998, PASP, 110, 3
Gonzalez O. A. et al., 2020, The Messenger, 180, 18
Grcevich J., Putman M. E., 2009, ApJ, 696, 385
Guelin M., Forestini M., Valiron P., Ziurys L. M., Anderson M. A., Cernicharo J., Kahane C., 1995, A&A, 297, 183
Gunn J. E. et al., 2006, AJ, 131, 2332
Harris C. R. et al., 2020, Nature, 585, 357
Hasselquist S. et al., 2017, ApJ, 845, 162
Hasselquist S. et al., 2019, ApJ, 872, 58
Hasselquist S. et al., 2019, ApJ, 872, 58
Hasselquist S. et al., 2021, ApJ, 923, 172
Hawkins K., Jofré P., Masseron T., Gilmore G., 2015, MNRAS, 453, 758
Hayes C. R. et al., 2018, ApJ, 852, 49
Hayes C. R. et al., 2020, ApJ, 889, 63
Haywood M., Di Matteo P., Lehnert M. D., Snaith O., Khoperskov S., Gómez A., 2018, ApJ, 863, 113
Helmi A., Babusiaux C., Koppelman H. H., Massari D., Veljanoski J., Brown A. G. A., 2018, Nature, 563, 85
Hendricks B., Koch A., Lanfranchi G. A., Boeche C., Walker M., Johnson C. I., Peñarrubia J., Gilmore G., 2014, ApJ, 785, 102
Hill V. et al., 2019, A&A, 626, A15
Hillebrandt W., Niemeyer J. C., 2000, ARA&A, 38, 191
Holtzman J. A. et al., 2015, AJ, 150, 148
Holtzman J. A. et al., 2018, AJ, 156, 125
Horta D. et al., 2020, MNRAS, 493, 3363
Horta D. et al., 2021a, MNRAS, 500, 1385
Horta D. et al., 2021b, MNRAS, 500, 1385
Horta D. et al., 2022a, MNRAS, in press
Horta D. et al., 2022b, MNRAS
Hunter J. D., 2007, Comput. Sci. Eng., 9, 90
Ibata R. A., Gilmore G., Irwin M. J., 1994, Nature, 370, 194
Iwamoto K., Brachwitz F., Nomoto K., Kishimoto N., Umeda H., Hix W. R., Thielemann F.-K., 1999, ApJS, 125, 439
Kamiński T. et al., 2018, Nat. Astron., 2, 778
Kobayashi C., Leung S.-C., Nomoto K., 2020, ApJ, 895, 138
Kobayashi C., Umeda H., Nomoto K., Tominaga N., Ohkubo T., 2006, ApJ, 653, 1145
Koppelman H. H., Helmi A., Massari D., Price-Whelan A. M., Starkenburg T. K., 2019, A&A, 631, L9
Kruijssen J. M. D. et al., 2020, MNRAS, 498, 2472
Lane J. M. M., Bovy J., Mackereth J. T., 2022, MNRAS, 510, 5119
Leung H. W., Bovy J., 2019, MNRAS, 489, 2079
Limongi M., Chieffi A., 2006, ApJ, 647, 483
Mackereth J. T. et al., 2019, MNRAS, 482, 3426
Mackereth J. T., Bovy J., 2018, PASP, 130, 114501
Mackereth J. T., Bovy J., 2020, MNRAS, 492, 3631
Mackereth J. T., Crain R. A., Schiavon R. P., Schaye J., Theuns T., Schaller M., 2018, MNRAS, 477, 5072
Majewski S. R. et al., 2013, ApJ, 777, L13
Majewski S. R. et al., 2017, AJ, 154, 94
Martin N. F., Ibata R. A., Chapman S. C., Irwin M., Lewis G. F., 2007, MNRAS, 380, 281
Massari D., Koppelman H. H., Helmi A., 2019, A&A, 630, L4
Matsuno T. et al., 2021, ApJ, 912, 72
Matteucci F., Greggio L., 1986, A&A, 154, 279
McConnachie A. W., 2012, AJ, 144, 4
McConnachie A. W., Venn K. A., 2020, Res. Notes Am. Astron. Soc., 4, 229
McMillan P. J., 2017, MNRAS, 465, 76
McWilliam A., 1997, ARA&A, 35, 503
Morris M., Serabyn E., 1996, ARA&A, 34, 645
Naidu R. P., Conroy C., Bonaca A., Johnson B. D., Ting Y.-S., Caldwell N., Zaritsky D., Cargile P. A., 2020, ApJ, 901, 48
Nataf D. M., 2017, Publ. Astron. Soc. Aust., 34, 41
Nidever D. L. et al., 2015, AJ, 150, 173
Nidever D. L. et al., 2020, ApJ, 895, 88
Nissen P. E., Schuster W. J., 2010, A&A, 511, L10
Nissen P. E., Schuster W. J., 2011, A&A, 530, A15
Nofar I., Shaviv G., Starrfield S., 1991, ApJ, 369, 440
Nomoto K., Thielemann F. K., Yokoi K., 1984, ApJ, 286, 644
Oliphant T., 2006, A Guide to NumPy. Trelgol Publishing, USA
Prantzos N., Diehl R., 1996, Phys. Rep., 267, 1
Rich R. M., 2013, in Oswalt T. D., Gilmore G., eds, Planets, Stars and Stellar Systems. Springer, Dordrecht, p. 271
Samland M., 1998, ApJ, 496, 155
Santana F. A. et al., 2021, AJ, 162, 303
Schiavon R. P. et al., 2022, MNRAS, submitted
Schuster W. J., Moreno E., Nissen P. E., Pichardo B., 2012, A&A, 538, A21
Shetrone M., Venn K. A., Tolstoy E., Primas F., Hill V., Kaufer A., 2003, AJ, 125, 684
Starkenburg E. et al., 2013, A&A, 549, A88
Steinmetz M. et al., 2006, AJ, 132, 1645
Taylor M. B., 2005, in Shopbell P., Britton M., Ebert M., eds, ASP Conf. Ser. Vol. 347, Astronomical Data Analysis Software and Systems XIV. Astron. Soc. Pac., San Francisco, p. 29
Theler R. et al., 2020, A&A, 642, A176
Virtanen P. et al., 2020, Nat. Methods, 17, 261
Walker M. G., Mateo M., Olszewski E. W., 2008, ApJ, 688, L75
Walker M. G., Mateo M., Olszewski E. W., 2009a, AJ, 137, 3100
Walker M. G., Mateo M., Olszewski E. W., Gnedin O. Y., Wang X., Sen B., Woodroofe M., 2007, ApJ, 667, L53
Walker M. G., Mateo M., Olszewski E. W., Peñarrubia J., Evans N. W., Gilmore G., 2009b, ApJ, 704, 1274
Weinberg D. H. et al., 2019, ApJ, 874, 102
Weiss A., Truran J. W., 1990, A&A, 238, 178
Wheeler J. C., Sneden C., Truran J. W. Jr, 1989, ARA&A, 27, 279
White S. D. M., Rees M. J., 1978, MNRAS, 183, 341
Wilkinson M. I., Kleyna J. T., Evans N. W., Gilmore G. F., Irwin M. J., Grebel E. K., 2004, ApJ, 611, L21
Wilson J. C. et al., 2019, PASP, 131, 055001
Woosley S. E., Weaver T. A., 1995, ApJS, 101, 181
Yanny B. et al., 2009, AJ, 137, 4377
Zasowski G. et al., 2013, AJ, 146, 81
Zasowski G. et al., 2017, AJ, 154, 198

This paper has been typeset from a TEX/LATEX file prepared by the author.